



RESEARCH ARTICLE

Glucose and mannose analogs inhibit KSHV replication by blocking *N*-glycosylation and inducing the unfolded protein response

Mariana Schlesinger^{1,2} | Christian McDonald^{1,2} | Anuj Ahuja^{1,2}  |
 Carolina Alejandra Alvarez Canete^{1,2} | Zelmira Nuñez del Prado^{1,2} |
 Julian Naipauer^{1,2,3,4}  | Theodore Lampidis^{1,5} | Enrique A. Mesri^{1,2,3,†}

¹Tumor Biology Program, Sylvester Comprehensive Cancer Center, Miami, Florida, USA

²Department of Microbiology and Immunology, Miami Center for AIDS Research, MIAMI, Florida, USA

³UM-CFAR/SCCC Argentina Consortium for AIDS Malignancies, Miami, Florida, USA

⁴Instituto de Fisiología, Biología Molecular y Neurociencias (IFIBYNE), CONICET-Universidad de Buenos Aires, Buenos Aires, Argentina

⁵Department of Cell Biology, University of Miami Miller School of Medicine, Miami, Florida, USA

Correspondence

Julian Naipauer, Instituto de Fisiología, Biología Molecular y Neurociencias (IFIBYNE), CONICET-UBA Pabellón IFIBYNE, Ingreso por Av. Costanera, Rafael Obligado-Ciudad Universitaria, CABA-Buenos Aires, Argentina.
 Email: juliannaipauer@gmail.com

Funding information

National Institutes of Health

Abstract

Kaposi's sarcoma-associated herpesvirus (KSHV) is the etiological agent for Kaposi's sarcoma (KS), an HIV/AIDS-associated malignancy. Effective treatments against KS remain to be developed. The sugar analog 2-deoxy-D-glucose (2-DG) is an anticancer agent that is well-tolerated and safe in patients and was recently demonstrated to be a potent antiviral, including KSHV and severe acute respiratory syndrome coronavirus 2. Because 2-DG inhibits glycolysis and *N*-glycosylation, identifying its molecular targets is challenging. Here we compare the antiviral effect of 2-DG with 2-fluoro-deoxy-D-glucose, a glycolysis inhibitor, and 2-deoxy-fluoro-D-mannose (2-DFM), a specific *N*-glycosylation inhibitor. At doses similar to those clinically achievable with 2-DG, the three drugs impair KSHV replication and virion production in iSLK.219 cells via downregulation of viral structural glycoprotein expression (K8.1 and gB), being 2-DFM the most potent KSHV inhibitor. Consistently with the higher potency of 2-DFM, we found that D-mannose rescues KSHV glycoprotein synthesis and virus production, indicating that inhibition of *N*-glycosylation is the main antiviral target using D-mannose competition experiments. Suppression of *N*-glycosylation by the sugar drugs triggers ER stress. It activates the host unfolded protein response (UPR), counteracting KSHV-induced inhibition of the protein kinase R-like endoplasmic reticulum kinase branch, particularly activating transcription factor 4 and C/EBP homologous protein expression. Finally, we demonstrate that sugar analogs induce autophagy (a prosurvival mechanism) and, thus, inhibit viral replication playing a protective role against KSHV-induced cell death, further supporting their direct antiviral effect and potential therapeutic use. Our work identifies inhibition of *N*-glycosylation leading to ER stress and UPR as an anti-enveloped virus target and sugar analogs such as 2-DG and the newly identified 2-DFM as antiviral drugs.

[†]Deceased, August 27, 2022.

KEYWORDS

2-deoxy-2-fluoro-D-mannose, 2-deoxy-D-glucose, 2-fluoro-deoxy-D-glucose, Kaposi's sarcoma herpesvirus, sugar analogs, unfolded protein response

1 | INTRODUCTION

Kaposi's sarcoma-associated herpesvirus (KSHV or HHV8) is the causative agent of Kaposi's sarcoma (KS), primary effusion B-cell lymphoma (PEL), multicentric Castlemann's disease (MCS), and two understudied inflammatory syndromes.^{1–3} KS occurs in the context of aging in specific ethnic populations due to chronic inflammation and transplant-associated immune suppression and is the most common cancer in HIV/AIDS patients. AIDS-KS incidence has decreased since the implementation of antiretroviral therapy (ART). Still, advanced and ART-resistant stages of the illness require systemic chemotherapy, to which most patients are unresponsive. With over 38 million people diagnosed with HIV/AIDS at the end of 2019 (UNAIDS), an increase in organ transplantations globally (147 000 in 2018 according to the GODT and WHO-ONT), and an expanding older population, there is a critical need to identify antivirals for prevention and treatment of KS. Thus, insights from knowledge of KSHV biology and oncogenesis should provide a platform for identifying and developing improved anti-KS therapies.

KSHV displays latency and lytic replication. Although KS lesions primarily consist of latently infected cells, most antiviral approaches target the lytic viral cycle.⁴ KSHV latent and lytic genes are responsible for oncogenicity through a mechanism known as paracrine oncogenesis, whereby angiogenic and pro-KS factors such as vascular endothelial growth factor and platelet-derived growth factor, produced by lytically infected cells, drive angiogenesis and proliferation of latently infected cells.⁵ Additionally, the perpetuation of viral infection depends on the completion of the lytic cycle. KSHV antivirals are thought to block KSHV replication, the spread of infection, and paracrine oncogenesis.

During KSHV late lytic replication, the massive production of viral structural components makes up the viral envelope. Glycoprotein gB has a conserved function for virion binding and entry and plays a role in viral maturation and virion egress.⁶ Glycoprotein K8.1 is expressed in multiple variants with different degrees of glycosylation (ranging from 26 to 72 kDa), with the mature form(s) on virions being highly glycosylated (68–72 kDa).⁷ Viral glycoproteins are mass-produced, modified, and folded in the endoplasmic reticulum (ER) and the Golgi apparatus.^{8–11} In uninfected cells, excessive glycoprotein synthesis typically triggers ER stress, and, as a consequence, the unfolded protein response (UPR) is activated to restore cell homeostasis. If ER protein homeostasis cannot be re-established, UPR switches from an adaptive to an apoptotic response. However, ER stress can also initiate autophagy. This important prosurvival mechanism counteracts excessive UPR signaling by compensating and assisting with a system known as endoplasmic reticulum-associated degradation (ERAD), producing bulk protein

degradation.¹² KSHV, like other viruses, deploys mechanisms that hijack these host cellular responses to support viral replication.

Based on phase I clinical trial results, the sugar analog 2-deoxy-D-glucose (2-DG) has been proposed as a cancer therapy adjuvant that is well-tolerated and safe in patients. Besides being currently studied as an investigational drug against cancer, in recent years, 2-DG has also been proposed as an antiviral agent acting through different mechanisms: by being pseudoincorporated into the structure of the viral capsid, by shutting off the building blocks required for viral replication through glycolysis inhibition,^{13,14} and, as previously shown by our research group, by interfering with normal glycoprotein synthesis via ER stress and UPR activation.^{8,15} Recently, a 2-DG oral formulation was approved in India for emergency use as an adjunct therapy to treat moderate to severe coronavirus disease of 2019 (COVID-19) patients.¹⁶ Moreover, it has been shown that 2-DG inhibits severe acute respiratory syndrome coronavirus 2 (SARS-CoV-2) multiplication in colon cancer cells.¹⁷

2-fluoro-deoxy-D-glucose (2-FDG) is another sugar analog of clinical importance that mimics D-glucose and, consequently, inhibits glycolysis with stronger potency than 2-DG.¹⁸ 2-DG and 2-FDG inhibition of glycolysis were cytotoxic in latently KSHV-infected cells only at high doses, not compatible with clinical use.¹³ Conversely, previous work from our research group showed that 2-DG, but not 2-FDG, interfered with KSHV replication and virion production at clinically achievable doses.⁸ We showed that during this process, 2-DG led to ER stress and activation of the host UPR, overwhelming the capacity of KSHV to deal with this cellular response during massive viral glycoprotein synthesis in the context of lytic replication.⁸ During the herpesvirus lytic phase, UPR is thought to be triggered by specific viral gene products rather than simply by overwhelming the ER folding capacity.^{9,11,19} McCormick et al. reported that all three ER-localized UPR sensors are activated following viral reactivation from latency in PEL cells. They also suggested that UPR activation is proviral and that KSHV hijacks this process to promote efficient viral replication rather than resolving ER stress. This assumption is based on KSHV-elicited inhibition of UPR downstream transcription factors, which are required to mitigate ER stress and restore ER homeostasis.¹² In summary, induction of ER stress by 2-DG seems to be a promising strategy against KSHV.¹⁵

A better understanding of the cellular mechanisms affected by 2-DG could offer new avenues for innovative therapies against KSHV. However, because 2-DG inhibits glycolysis and N-glycosylation, it is challenging to identify its molecular targets. For this reason, we added to our study the D-mannose analog 2-deoxy-2-fluoro-D-mannose (2-DFM), which exerts a more specific effect on N-glycosylation obstruction than the other two drugs. Briefly, 2-DG is structurally equivalent to 2-deoxy-D-mannose and, therefore, can be

incorporated into the 14-sugar precursor (Glc₃Man₉GlcNAc₂-P-P-Dolichol) that is cotranslationally added to the nascent polypeptide in the ER during *N*-glycosylation, leading to its premature termination. Also, intracellular conjugation of 2-DG to guanosine diphosphate or dolichol phosphate depletes these *D*-mannose-activating precursors, further disrupting normal oligosaccharide formation.²⁰ 2-FDG does suppress *N*-glycosylation, albeit with significantly lower potency than 2-DG. It indirectly inhibits this posttranslational modification by decreasing the metabolites necessary for *D*-mannose transport from the cytosol into the ER and directly by competing for the glucose added at the end of the 14-sugar precursor assembly.²¹ 2-DFM suppresses *N*-glycosylation by inhibiting mannosyl transferases indispensable for *D*-mannose incorporation into the 14-sugar precursor.²⁰ Unlike 2-DG, however, it cannot be incorporated into this oligosaccharide chain and, therefore, the order of potency in disrupting *N*-glycosylation is 2-DG > 2-DFM > 2-FDG.^{20,22,23}

In the present study, we sought to molecularly characterize and systematically compare the antiviral capacities of 2-DG, 2-FDG, and 2-DFM. These sugar analogs allowed us to study their antiviral effect based on their potency and specificity (inhibitors of glycolysis vs. *N*-glycosylation). This work identified sugar analogs' nontoxic inhibition of *N*-glycosylation as a critical antiviral target. It showed that disruption of this process invokes a more potent inhibition of KSHV replication at lower doses, similar to those clinically achievable with 2-DG. Our further characterization of drug-elicited responses to ER stress and UPR activation also revealed the protective role, via autophagy, that the sugar analogs play in cellular hosts where KSHV undergoes lytic replication. Finally, our data point out a novel compound—2-DFM—as a more specific *N*-glycosylation suppressor and, thus, a more potent inhibitor of KSHV replication and reinforce the potential of 2-DG as a drug against KSHV and other enveloped viruses, such as SARS-CoV-2.

2 | MATERIALS AND METHODS

2.1 | Cell culture and constructs

We studied the oncovirus KSHV: *Herpesvirales Herpesviridae Gammaherpesvirinae Rhadinovirus Human gammaherpesvirus 8*. The KSHV producer cell line iSLK.219 harbors a recombinant virus (rKSHV.219) that contains green fluorescent protein (GFP) (infection marker) under the control of the human EF1- α promoter and red fluorescent protein (RFP) (reactivation marker) under the control of the KSHV lytic polyadenylated nuclear (PAN) promoter (Figure 1A).²⁴ The KSHV producer cell line iSLK.BAC16 harbors a recombinant virus (rKSHV.BAC16) that contains GFP (infection marker) under the control of the human EF1- α promoter.²⁵ The KSHV producer cell line iSLK.BAC16 (RGB) harbors a recombinant virus (rKSHV.BAC16 [RGB]) that contains RFP (infection marker) under the control of the human EF1- α promoter, GFP (early lytic reactivation marker) under the control of the KSHV lytic PAN promoter, and blue fluorescent protein (BFP) (late lytic reactivation marker) under the

control of the KSHV lytic K8.1 promoter.²⁶ KSHV reactivation system expresses a doxycycline (DOX)-inducible replication and transcription activator (RTA) (KSHV ORF50) transgene to trigger the lytic switch, which can be further potentiated by adding the histone deacetylase inhibitor sodium butyrate.²⁷

iSLK (KSHV-negative) cells, iSLK.219 (rKSHV.219) cells, iSLK-BAC16 (rKSHV.BAC16), iSLK.BAC16 (RGB) (rKSHV.BAC16 RGB), and HEK-AD293 cells were cultured in Dulbecco's modified Eagle medium containing 10% fetal bovine serum (Gemini Bio-Products) and 1% penicillin-streptomycin (Gibco). iSLK cells were cultured in the presence of 10 μ g/ml puromycin (Gibco) and 800 μ g/ml G418 (Sigma). iSLK.219 (rKSHV.219) cells were cultured in presence of 1 μ g/ml puromycin, 800 μ g/ml G418, and 1.2 mg/ml hygromycin B (Invitrogen).²⁷ iSLK.BAC16 (RGB) and iSLK.BAC16 cells were cultured in the presence of 1 μ g/ml puromycin, 250 μ g/ml G418, and 1.2 mg/ml hygromycin B.

2.2 | Lytic induction and 50% tissue culture infective dose

iSLK.219 cells were induced at 60% confluency with DOX (1 μ g/ml, Sigma-Aldrich) and sodium butyrate (1 mM) in the absence (–) or presence of one of the sugar analogs: 2-DG (Sigma), 2-FDG (Carbosynth), and 2-DFM (Carbosynth) at 2 or 5 mM. After 72 h of induction, cell-free virus-containing supernatants were collected and, after a serial dilution, were used to de novo infect HEK-AD293, which were pretreated for 30 min with 8 μ g/ml polybrene (Millipore). A total of 72 h after infection, infectious virion production was measured by counting the GFP+ HEK-AD293 by flow cytometry to determine the 50% tissue culture infective dose (1 GFP(+) AdHEK293 cell = 1 infectious KSHV virion).

2.3 | Western Blotting

Radioimmunoprecipitation assay lysis buffer (Thermo Fisher Scientific) containing phosphatase and protease inhibitors (Sigma) was used to obtain protein lysates. These lysates were sonicated and centrifuged at 10 000 rpm for 10 min to remove genomic DNA. Protein concentration was measured using a bicinchoninic acid assay protein assay (Thermo Fisher Scientific) before adding Laemmli buffer (Bio-rad) containing β -mercaptoethanol to the samples. An equal amount of protein was loaded and resolved in a gradient SDS-PAGE gel (Bio-rad). The gel was transferred to a polyvinylidene difluoride membrane (Bio-rad) and was blocked with 3% BSA (Sigma) to reduce nonspecific binding. Membranes were incubated with primary antibodies diluted in 1% BSA overnight. We used the following antibodies: KSHV latency-associated nuclear antigen (LANA) (Abcam), KSHV ORF45 (Thermo Fisher Scientific), KSHV K8.1 (Santa Cruz Biotechnology), KSHV gB (Thermo Fisher Scientific), KSHV RTA (ABBIOTEC), KSHV ORF57 (Santa Cruz Biotechnology), KSHV ORF26 monoclonal antibody (2F6B8) (Thermo Fisher

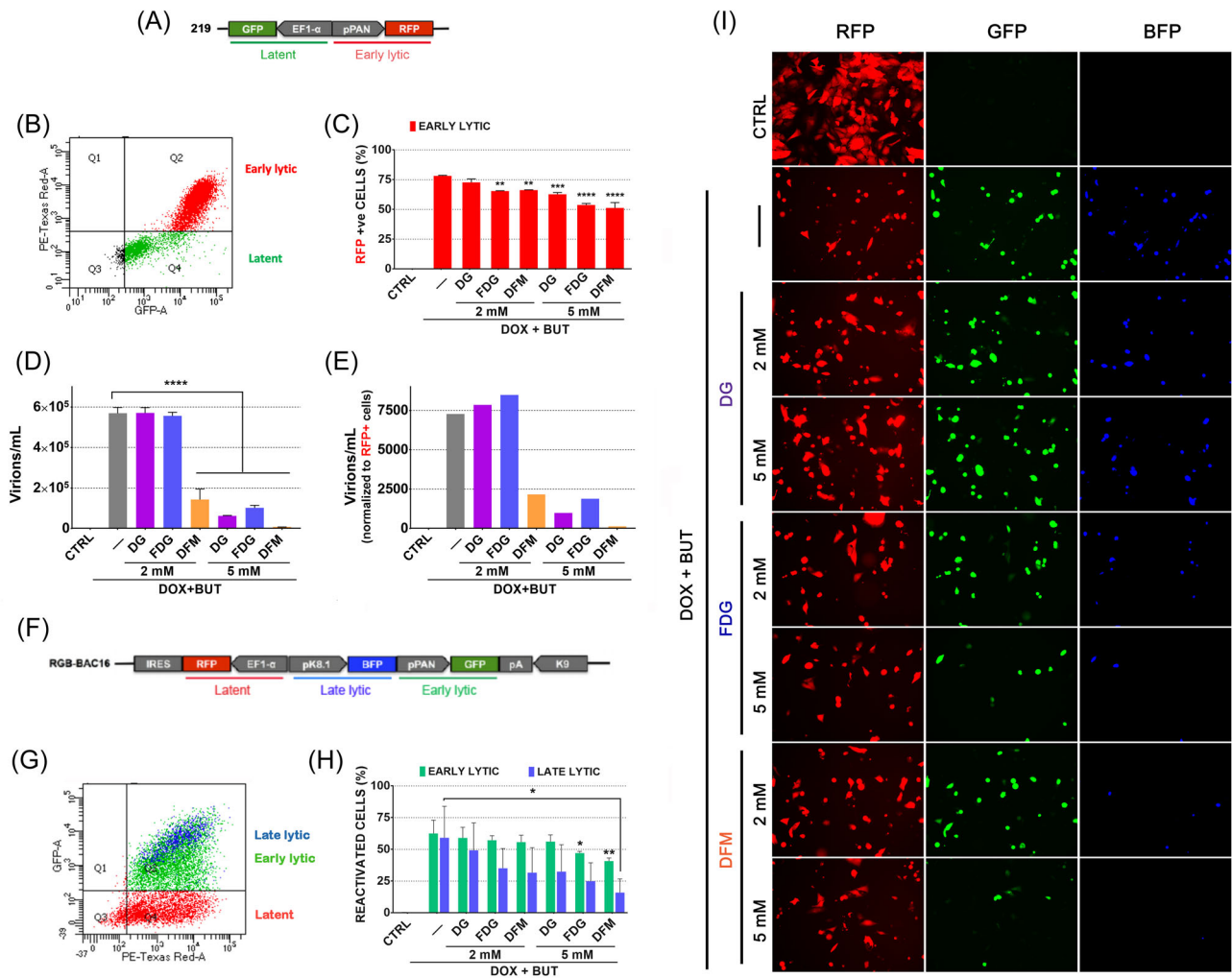


FIGURE 1 2-DG, 2-FDG, and 2-DFM reduce the virus titers of reactivated iSLK.219 cells. KSHV-infected cells were reactivated with doxycycline (1 μ g/ml) and sodium butyrate (BUT) (1m the M) in the absence (–) or presence of one of the sugar analogs: 2-DG, 2-FDG, and 2-DFM at 2 or 5 mM. Nonreactivated cells were used as a control (CTRL). (A) Schematic diagram of the construct that bears the recombinant virus rKSHV.219, which expresses the green fluorescent protein (GFP) from the EF-1 α promoter to identify infected cells, and the red fluorescent protein (RFP) from the strong KSHV lytic PAN promoter (directly activated by RTA) to identify reactivated cells. (B) A representative flow cytometry plot of how GFP-positive cells (infected) and RFP-positive cells (early lytically reactivated) were detected by flow cytometry 48 h after reactivation of iSLK.219 cells. (C) RFP-positive (early lytically reactivated) iSLK.219 cells were quantified 48 h postreactivation by flow cytometry, as shown in (B). The average of two independent experiments is graphed. (Mean \pm SD; ** p < 0.002; *** p < 0.001; **** p < 0.0001; One-way ANOVA and Dunnett's multiple comparisons test). (D) To measure the virus titer, virus-containing supernatants from iSLK.219 cells were serially diluted and spinoculated onto a monolayer of AdHEK293 cells. GFP-positive cells (infected) were quantified by flow cytometry after 72 h of de novo infection and virus titers (virions/ml) were calculated (1 GFP (+) AdHEK293 cell = 1 infectious KSHV virion). Values were performed in triplicates and presented as means \pm SD (**** p < 0.0001; One-way ANOVA and Dunnett's multiple comparisons test). (E) Virus titers (from D) were normalized to RFP-positive (reactivated) iSLK.219 cells (from C). (F) Schematic diagram of the construct that bears the recombinant virus rKSHV.BAC16 (RGB), which expresses the RFP from the EF-1 α promoter to identify infected cells, the GFP from the strong KSHV lytic PAN promoter (directly activated by RTA) to identify early lytically reactivated cells, and the blue fluorescent protein (BFP) from the K8.1 promoter to identify late lytically reactivated cells. (G) A representative flow cytometry plot of how RFP-positive cells (infected), GFP-positive cells (early lytically reactivated), and BFP-positive cells (late lytically reactivated) were detected by flow cytometry 48 h after reactivation of iSLK. BAC16 (RGB) cells. (H) GFP-positive cells (early lytically reactivated) and BFP-positive cells (late lytically reactivated, normalized to the number of early lytically reactivated cells) were quantified 48 h postreactivation by flow cytometry, as shown in (G). The average of two independent experiments is graphed. (Mean \pm SD; ** p < 0.002; *** p < 0.001; **** p < 0.0001; one-way ANOVA and Dunnett's multiple comparisons test). (I) Fluorescent images of iSLK.BAC16 (RGB) cells were acquired 48 h after reactivation and treatment with the sugar analogs with the ZOE Fluorescent Cell Imager. ANOVA, analysis of variance; KSHV, Kaposi's sarcoma-associated herpesvirus; PAN, polyadenylated nuclear; RTA, replication and transcription activator; 2-DG, 2-deoxy-D-glucose; 2-DFM, 2-deoxy-2-fluoro-D-mannose; 2-FDG, 2-fluoro-deoxy-D-glucose.

Scientific). All UPR markers are from cell signaling (binding immunoglobulin protein [BiP], protein kinase R-like endoplasmic reticulum kinase [PERK], phospho-PERK, phospho-eIF2a, eIF2a, activating transcription factor 4 [ATF4], C/EBP homologous protein [CHOP], activating transcription factor 6 [ATF6], IRE1a, and sXBP-1) as well as apoptotic and autophagic markers: p53, phospho P53, cleaved caspase 3, and LC3B(D11). Acetyl Histone H3 and Histone H3 (cell signaling), Actin (Sigma), and glyceraldehyde-3-phosphate dehydrogenase (Santa Cruz Biotechnology). Protein bands were visualized using SuperSignal West Pico PLUS Chemiluminescent Substrate (Thermo Fisher Scientific).

2.4 | Flow cytometry

To measure the amount of infected (GFP+) cells for the HEK-AD293 cell line, the amount of latent (GFP+) and lytically reactivated (GFP+/RFP+) cells for the iSLK.219 cell line or the amount of latent (RFP+), early lytically reactivated (RFP+/GFP+), and late lytically reactivated (RFP+/GFP+/BFP+) cells for the iSLK.BAC16 (RGB) cell line cells were washed 2X with 1X phosphate buffered saline (PBS) and fixed with 4% paraformaldehyde. We used VivaFix 410/450 (Bio-rad 135-1112) per manufacturer instructions for cell viability measurement. Flow cytometry analysis was performed using a Becton-Dickinson LSR analyzer (BD Biosciences).

2.5 | Quantification of intracellular and extracellular KSHV genomic DNA

After 72 h of lytic reactivation of iSLK.219 cells and viral loads (KSHV DNA copy numbers) were determined by real-time quantitative polymerase chain reaction (PCR). To quantify intracellular KSHV DNA copy number, supernatants were removed, and cells were lysed with trypsin ethylenediaminetetraacetic acid (Thermo Fisher Scientific). Trypsinization was halted with new media and centrifuged at 1000 rpm for 5 min. Pellets containing the cells were resuspended in 1X PBS to a final volume of 200 μ l. We added 20 μ l of proteinase K (QIAGEN protease) and followed the spin protocol per the manufacturer's instructions (DNA purification from blood or body fluids, QIAGEN; 51104). Intracellular viral DNA was calculated by quantitative PCR (qPCR) using the KSHV LANA gene and the cellular actin gene as a reference for normalization. To quantify extracellular KSHV DNA, supernatants were collected and filtered through 0.45 μ m filters. Cell-free supernatants were collected to de novo infect naïve HEK-AD293 cells, and 300 μ l were isolated to measure viral DNA. Before adding proteinase K (QIAGEN protease), we treated the samples with DNase I to eliminate the viral DNA that was not inside the virion. We followed the spin protocol per the manufacturer's instructions (DNA purification from blood or body fluids, QIAGEN; 51104).

2.6 | Real-time quantitative PCR

RNA was extracted from cells using RLT buffer (RNeasy Kit QIAGEN) containing β -mercaptoethanol. To remove DNA, samples were treated with RNase-Free DNase I (QIAGEN) on columns for 25 min at room temperature. RNA was reverse-transcribed into cDNA using ImProm-II Reverse Transcriptase (Promega) as directed by the manufacturer's protocol. Viral and host messenger RNA (mRNAs) were amplified using specific primers diluted in the SYBR green PCR master mix (Quanta Biosciences). The primer sets (Sigma) that were used are the following: actin forward 5'-CTCTCCAGCCTTCCTCCTG-3', actin reverse 5'-CAGCACTGTGTTGGCGTACAG-3', KSHV LANA forward 5'-CCTGGAAGTCCCACAGTGT-3', KSHV LANA reverse 5'-AGACA CAGGATGGGATGGAG-3'. For detection, we used the Atila machine and software. Nonreverse transcriptase and water controls were used to confirm the samples' absence of viral DNA and contamination. Actin was used as a housekeeping gene to perform the $\Delta\Delta$ CT method. The expression of viral genes was normalized to actin CT value, and the difference between viral CT values with actin was considered the Δ CT value. The obtained Δ CT values were normalized to a given control sample ($\Delta\Delta$ CT value), and the fold change was calculated using the $2^{-\Delta\Delta$ CT} formula.

2.7 | Cell proliferation assay (IncuCyte)

iSLK.BAC16 cells were plated at 8000 cells/well in a 96-well plate in triplicates. The next day all cells, except for the control cells, were induced with DOX (1 μ g/ml, Sigma) and sodium butyrate (1 mM) alone or in addition to one of the sugar analogs: 2-DG (Sigma), 2-FDG (Carbosynth), or 2-DFM (Carbosynth) at 5 mM. Additionally, a Cytotox Red Reagent at 250 nM (Essen Bioscience) was added to all wells. Cells were incubated in an IncuCyte Zoom (Essen Bioscience) to acquire green and red fluorescence images at 10X magnification every 4 h. The death index was calculated for each data point with the formula: red object count (dead cells)/green object count (iSLK.BAC16 cells).

2.8 | Microscopy

Images of iSLK.BAC16 (RGB) cells were acquired with ZOE Fluorescent Cell Imager (Bio-Rad) 48 h after reactivation with DOX (1 μ g/ml) and sodium butyrate (1 mM) in the absence (-) or presence of one of the sugar analogs: 2-DG (Sigma), 2-FDG (Carbosynth), and 2-DFM (Carbosynth) at 2 or 5 mM.

2.9 | Immunofluorescence

iSLK.219 cells were plated at a concentration of 2.5×10^4 cells/well in Labteks 24 h after reactivation and treatment with the analog

drugs (5 mM); cells were washed with 1X PBS and fixed with cold acetone for 20 min at -20°C . After discarding the acetone, cells were dried and stored at -20°C . Cells were washed with 1X PBS, dried, and incubated with the primary antibody (LC3B(D11), cell signaling, 3868) for 30 min at 37°C at a 1/40 dilution (in 1% milk). After a second wash with 1X PBS, cells were incubated with the secondary antibody Cy5 goat antirabbit IgG (H + L) (Invitrogen; A10523) for 30 min at 37°C at a 1/1600 dilution (in 1% milk). After the third wash with 1X PBS, cells were dried and the slides were mounted using the mounting solution ProLong gold antifade reagent with 4',6-diamidino-2-phenylindole (LifeTechnologies; P36931). Samples were analyzed using a Zeiss Axio Observer Z1 microscope and AxioVision software. Representative images were acquired with Leica DMI6000B microscope with LASX software (Leica).

2.10 | Statistical analysis

The statistical significance of all collected data was calculated using one-way analysis of variance with Dunnett's multiple comparisons posttest using GraphPad Prism 8 software. Values were performed in duplicates or triplicates and expressed as means \pm standard deviation.

3 | RESULTS

3.1 | Anti-KSHV replication effects of D-mannose and D-glucose sugar analogs

Our first aim was to compare the antiviral effect of the sugar analogs 2-DG, 2-FDG, and 2-DFM on KSHV viral replication. To this end, we first determined the ability of each drug to inhibit KSHV reactivation. We used the KSHV producer cell line iSLK.219 harboring a recombinant virus (rKSHV.219) that contains an infection marker (GFP) and a reactivation marker (RFP) (Figure 1A).²⁴ Figure 1B shows a representative flow cytometry plot of how GFP-positive cells (infected) and RFP-positive cells (early lytically reactivated) were detected and measured by flow cytometry 48 h after reactivation of iSLK.219 cells (Figure 1B). We found that at 2 mM, only 2-FDG and 2-DFM inhibited KSHV lytic reactivation leading to a 15% reduction in the number of reactivated cells. However, at 5 mM, the three sugar analogs inhibited KSHV lytic reactivation, albeit at different extents, with 2-FDG and 2-DFM reaching a 30% reduction (Figure 1C). At these pharmacologically active concentrations, the three drugs proved to be nontoxic (Figure S1).

Since all sugar analog treatments reduced the number of reactivated cells, we next sought to determine their impact on virion production. We assessed the infective capacity of supernatants from induced iSLK.219 cells using AdHEK293 cells (Figure 1D,E). At 2 mM concentration, only 2-DFM displayed a significant reduction in infectivity. However, all analog drugs significantly reduced virus titers at the highest concentration (5 mM), 2-DFM presenting the most potent antiviral effect abolishing the infective capacity of

virions from reactivated iSLK.219 cells. Our data show that while all these D-glucose and D-mannose analogs exhibit anti-KSHV activity, the D-mannose analog 2-DFM appears to be the most potent antiviral drug.

3.2 | 2-DG, 2-FDG, and 2-DFM inhibit virion production through downregulation of the structural late lytic glycoproteins K8.1 and gB

To dissect the level at which these drugs could exert their antiviral effects, we analyzed different processes after KSHV reactivation. We evaluated whether late lytic replication was also impaired by using the KSHV producer cell line iSLK.BAC16 (RGB) harbors a recombinant virus (rKSHV.BAC16 RGB). It contains an infection marker (RFP), an early reactivation marker (GFP), and a late lytic reactivation marker (BFP),²⁶ the latter being expressed from the K8.1 promoter (Figure 1F). Figure 1G shows a representative flow cytometry plot of how RFP-positive cells (infected), GFP-positive cells (early lytically reactivated), and BFP-positive cells (late lytically reactivated) were detected and measured by flow cytometry 48 h after reactivation of iSLK.BAC16 (RGB) cells (Figure 1G). Only 2-DFM inhibits early lytic and late reactivation at 5 mM (Figure 1H,I).

Next, we aimed to explore the effects of drugs on the production of KSHV glycoproteins that make up the viral envelope. We showed the expression levels of K8.1 and gB, which are mass-produced, modified, and folded in the ER/Golgi apparatus where N-glycosylation occurs. All three sugar analogs downregulated K8.1 expression dose-dependently 48 h after reactivation (Figure 2A). The most potent effect was observed with 2-DFM, followed by 2-FDG and 2-DG, and at 5 mM, 2-DFM abolished the expression of K8.1. We also found an acute reduction in glycoprotein gB expression when cells were subjected to the drug treatments. Drug-induced expression inhibition targets the late lytic glycoproteins since LANA (latent), ORF57 (early lytic), and ORF26 (late lytic protein of the capsid) expression levels remained unaltered with all treatments (Figures 2A and S2A). Moreover, we confirmed the specific glycoprotein downregulation by statistical analysis of K8.1 and LANA protein expression (Figure S2B).

Additionally, we measured the number of progeny KSHV DNA copies that occur intracellularly or in supernatants after virion release (Figure 2B,C). We quantified the intracellular KSHV genome copy number in reactivated cells by qPCR using the KSHV LANA gene and the cellular actin gene for normalization (Figure 2B). There was no significant difference in the amount of KSHV copies between untreated and treated cells with the sugar analogs, indicating that the drugs did not affect viral DNA replication. On the contrary, when we quantified the extracellular capsid-protected viral genomes in supernatants, we found that the three drugs significantly lowered the amount of KSHV DNA copies at 5 mM (Figure 2C). These results suggest that 2-DG, 2-FDG, and 2-DFM target a process after viral genome replication. These data mirror the disruption of late lytic glycoprotein expression shown previously (Figure 2A).

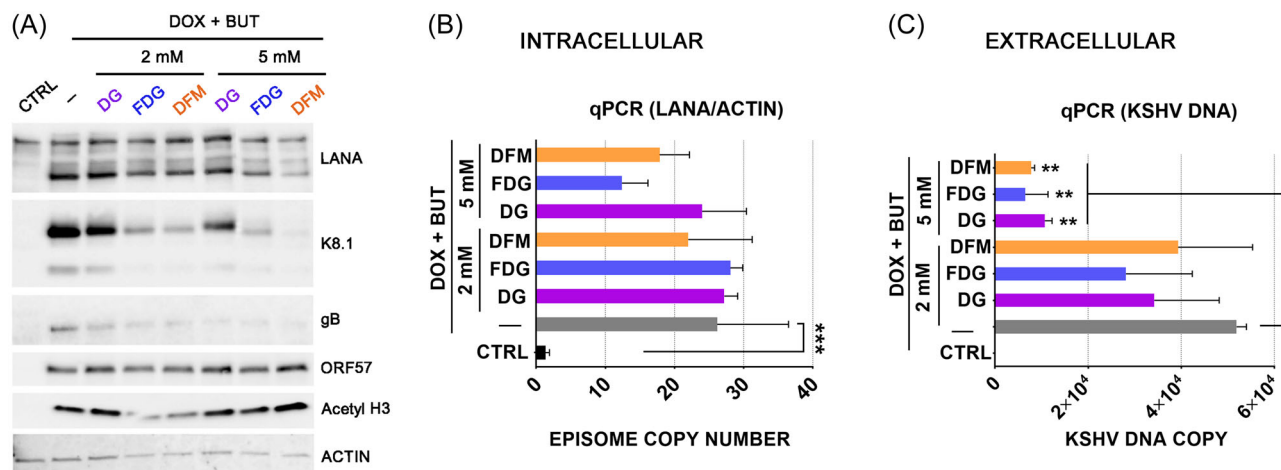


FIGURE 2 2-DG, 2-FDG, and 2-DFM inhibit virion production via downregulation of major viral structural glycoproteins. KSHV-infected iSLK.219 cells were reactivated with doxycycline (1 μ g/ml) and sodium butyrate (BUT) (1 mM) in the absence (–) or presence of one of the sugar analogs: 2-DG, 2-FDG, and 2-DFM at 2 or 5 mM. Nonreactivated cells were used as a control (CTRL). (A) Whole-cell lysates from iSLK.219 cells were analyzed at 48 h by immunoblots for KSHV proteins: LANA (latency gene), K8.1 (late lytic gene), gB (late lytic gene), ORF57 (early lytic gene), and acetyl-histone 3 (used as a control of sodium butyrate treatment, which reactivates the virus). β -actin was used as a loading control. The immunoblot shown here is representative of three independent experiments. (B) The intracellular KSHV DNA copy number was calculated by qPCR using the KSHV LANA gene and the $\Delta\Delta$ CT method with cellular β -actin as a reference gene for normalization. Samples were taken 72 h after reactivation of iSLK.219 cells and values were performed in triplicates and presented as means \pm SD (** p < 0.01; one-way ANOVA and Dunnett's multiple comparisons test). (C) Extracellular viral DNA was quantified by purifying capsid-protected genomic DNA from iSLK.219 cell supernatants and qPCR using the KSHV LANA gene with a KSHV BAC16 standard curve. Values were performed in triplicates and presented as means \pm SD (* p < 0.1; one-way ANOVA and Dunnett's multiple comparisons test). ANOVA, analysis of variance; KSHV, Kaposi's sarcoma-associated herpesvirus; LANA, latency-associated nuclear antigen; 2-DG, 2-deoxy-D-glucose; 2-DFM, 2-deoxy-2-fluoro-D-mannose; 2-FDG, 2-fluoro-deoxy-D-glucose.

Altogether, the three sugar drugs significantly diminished the virus titers of reactivated cells by lowering the expression of K8.1 and gB, which correlated to a lower number of virus particles in supernatants. On the other hand, despite lytic reactivation being negatively affected by the drugs, it did not impair viral episome replication or the expression of viral early lytic proteins.

3.3 | 2-DG, 2-FDG, and 2-DFM inhibit the expression of viral glycoproteins through N-glycosylation disruption

We performed D-mannose rescue experiments to confirm that the sugar analogs inhibit viral K8.1 and gB synthesis through N-glycosylation disruption (Figure 3). N-glycosylation occurs in the ER and needs the formation of a dolichol-linked precursor (Glc₃Man₉GlcNAc₂-P-P-Dolichol), distributed on three extended mannose branches. D-mannose is, therefore, an essential compound in this process. We added increasing D-mannose concentrations to reactivated cells to rescue the phenotype observed with the drug treatments (Figure 3A,B). Downregulation of glycoproteins gB and K8.1 was completely reversed by D-mannose in a dose-dependent manner with the three sugar analogs 2-DG, 2-FDG, and 2-DFM. With 2-DG, however, the reversion was weaker for gB. These results demonstrate that 2-DG, 2-FDG, and 2-DFM decrease viral glycoprotein synthesis in the ER via N-glycosylation suppression.

We next inquired whether the re-establishment of glycoprotein synthesis with D-mannose was enough to restore the infective capacity of KSHV virions. We measured the virus titers of reactivated cells treated with the sugar analogs in different concentrations of D-mannose (Figure 3C). The low virus titers due to drug treatments were fully rescued by D-mannose in a concentration-dependent manner. Even the 2-DFM's most potent inhibitory effect could be counteracted. Importantly, the low virus titers were fully rescued at higher concentrations of D-mannose. As expected, adding D-mannose alone did not result in higher virus titers (green bars, Figure 3C). Conversely, D-mannose could not reverse the reduced number of lytically reactivated cells caused by sugar analog treatments (Figure 3D).

In summary, our data show that the analog drugs reduce the infective capacity of virions by downregulating viral glycoproteins and point out N-glycosylation suppression as the main contribution of their inhibitory effect.

3.4 | The analog drugs activate the UPR in uninfected iSLK cells

We hypothesized that the disruption of N-glycosylation generated by the sugar analogs would likely trigger ER stress and, thus, activate intracellular signaling transduction pathways collectively termed UPR. To confirm this hypothesis, we examined the

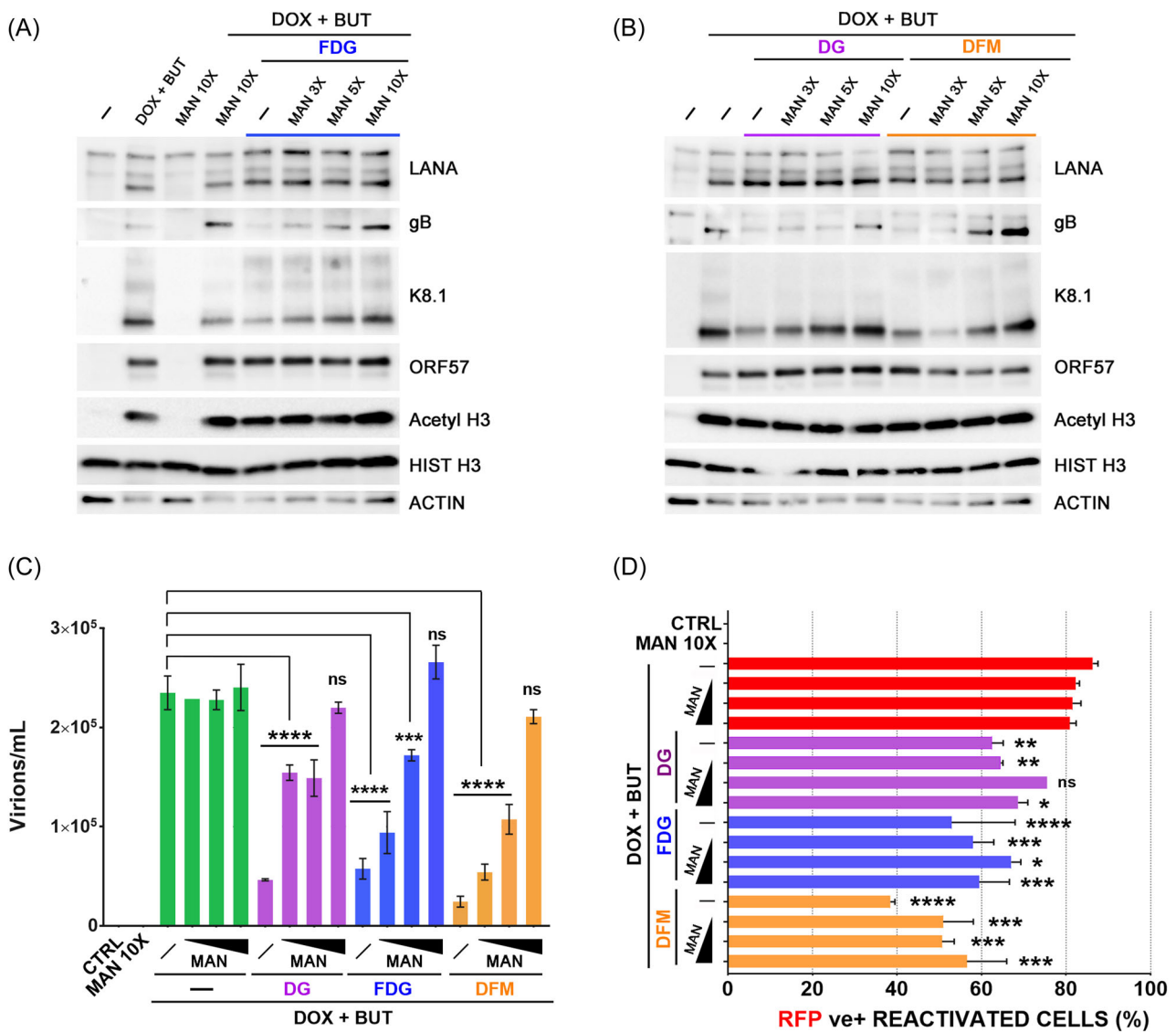


FIGURE 3 D-mannose reverses the inhibition of virion infectivity and the downregulation of viral lytic glycoprotein expression but does not reverse the inhibition of lytic reactivation. Induced iSLK.219 cells (DOX + BUT), reactivated with doxycycline (1 μ g/ml) and sodium butyrate (1 mM), were treated with one of the sugar analogs 2-DG, 2-FDG, or 2-DFM (3 mM), alone (–) or in addition to D-mannose (MAN) (3X: 9 mM; 5X: 15 mM; 10X: 30 mM), which was added 10 min before induction/treatment. (A, B) Whole-cell lysates were analyzed 72 h postinduction/treatment (drugs used at 3 mM) by immunoblots for the KSHV proteins: LANA (latent gene), gB (late lytic gene), K8.1 (late lytic gene), and ORF57 (early lytic gene). Histone H3 (HIST H3) and Acetyl-Histone H3 (Acetyl-H3) were used as a control of sodium butyrate treatment (which reactivates the virus) and β -actin (actin) as a loading control. (C) Virus titers were quantified from induced iSLK.219 cells were treated with 5 mM sugar analogs and D-mannose (MAN) (3X: 15 mM; 5X: 25 mM; 10X: 50 mM), which was added 10 min before induction/treatment. Virus-containing supernatants were serially diluted and spinoculated onto a monolayer of AdHEK293 cells. GFP-positive cells (infected) were quantified by flow cytometry after 72 h of de novo infection and virus titers (virions/ml) were calculated (1 GFP(+) AdHEK293 cell = 1 infectious KSHV virion). Values were performed in duplicates and presented as means \pm SD (** $p < 0.001$; **** $p < 0.0001$; one-way ANOVA and Dunnett's multiple comparisons test). (D) RFP-positive (early lytically reactivated) iSLK.219 cells were quantified 48 h after reactivation/treatment (drugs used at 3 mM) by flow cytometry. An average of two independent experiments are graphed. (Mean \pm SD; * $p < 0.05$; ** $p < 0.01$; *** $p < 0.001$; **** $p < 0.0001$; One-way ANOVA and Dunnett's multiple comparisons test). ANOVA, analysis of variance; GFP, green fluorescent protein; KSHV, Kaposi's sarcoma-associated herpesvirus; LANA, latency-associated nuclear antigen; 2-DG, 2-deoxy-D-glucose; 2-DFM, 2-deoxy-2-fluoro-D-mannose; 2-FDG, 2-fluoro-deoxy-D-glucose.

activation of stress-induced UPR sensors and their downstream effectors. Briefly, UPR is initiated by three ER-localized integral membrane proteins: Protein kinase RNA (PKR)-like endoplasmic reticulum kinase (PERK), ATF6, and inositol-requiring enzyme 1 (IRE1t are typically maintained in an inactive state by the

abundant ER chaperone immunoglobulin heavy chain-binding protein (BiP; also known as glucose-regulated protein, 78 kDa, GRP78).²⁸ PERK phosphorylates eIF2 α , which attenuates bulk translation and causes the selective translation of the transcription factor ATF4 and its downstream target transcription factor

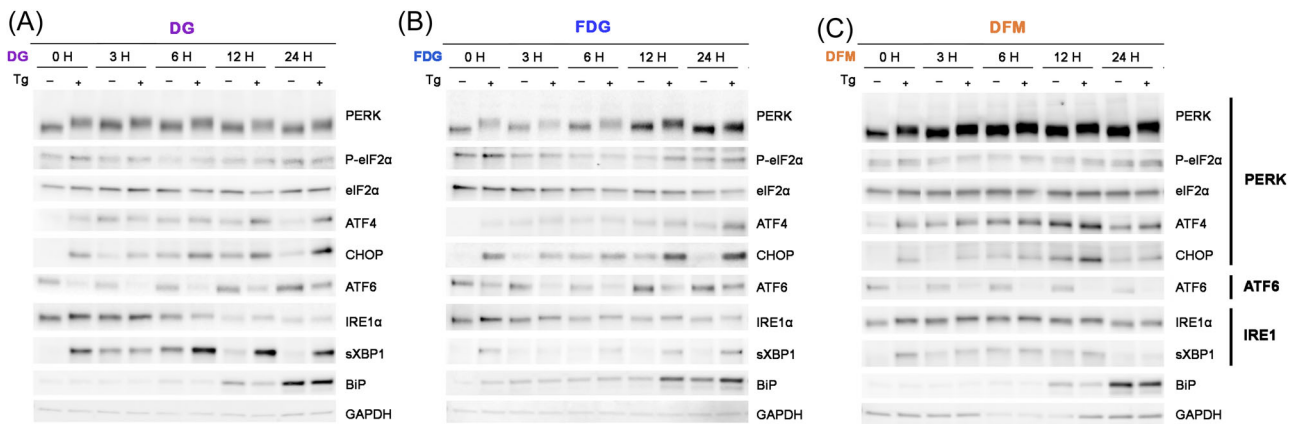


FIGURE 4 All analog drugs activate two branches of the unfolded protein response (UPR) in uninfected iSLK cells. UPR markers (PERK, phospho- and total eIF2 α , ATF4, CHOP, full-length ATF6, IRE1 α , sXBP-1, and BiP) were analyzed. Migration shift in PERK and IRE1 α immunoblots correspond to phosphorylation. GAPDH was used as a loading control. Whole-cell lysates from uninfected iSLK cells were analyzed by immunoblots at different hours posttreatment (H) with 2-DG (A), 2-FDG (B), or 2-DFM (C) at 5 mM. As a positive control of UPR activation, cells were treated with 150 nM thapsigargin (Tg) for 4 h before harvest. ATF6, activating transcription factor 6; BiP, binding immunoglobulin protein; CHOP, C/EBP homologous protein; GAPDH, glyceraldehyde-3-phosphate dehydrogenase; PERK, protein kinase R-like endoplasmic reticulum kinase; 2-DG, 2-deoxy-D-glucose; 2-DFM, 2-deoxy-2-fluoro-D-mannose; 2-FDG, 2-fluoro-deoxy-D-glucose.

CHOP. ATF6 translocates to the Golgi, which is proteolytically cleaved, releasing the N-terminal cytoplasmic transcription factor ATF6-N. IRE1 is a kinase and endoribonuclease that splices out a 26-nucleotide intron on XBP1 mRNA, which causes a translational frameshift to generate the transcription factor sXBP1. ATF6-N, sXBP1, and ATF4 transactivate genes involved in protein folding, degradation of misfolded proteins, lipid synthesis, and antioxidant responses.

We analyzed the expression levels of UPR markers at different time points after adding the sugar analogs (0, 3, 6, 12, and 24 h) in uninfected iSLK cells (Figure 4). As a positive control of UPR activation for each time point, we used the SERCA (sarco/ER Ca²⁺-ATPase) inhibitor thapsigargin (Tg) to pharmacologically induce ER stress. As expected, 2-DG, 2-FDG, and 2-DFM triggered two of the three UPR downstream pathways. PERK was activated (assessed by its subtle migration due to PERK phosphorylation, Figure 4 and S3A,B), and the downstream transcription factors ATF4 and CHOP were expressed 3 or 6 h after sugar analog treatments, almost to the same extent as treatment with Tg (Figure 4). Strikingly, eIF2 α phosphorylation levels did not change over time, indicating that an alternative factor may activate the ATF4/CHOP axis, such as eIF2A.²⁸ Also, IRE1 α was triggered (assessed by its subtle migration), and its downstream transcription factor sXBP1 was expressed 3 h after treatment (Figures 4 and S3A). However, activation of the ATF6 branch does not seem to be triggered by any sugar analog (Figures 4 and S3A). Finally, chaperone BiP/GRP78 was upregulated 12 h after 2-DG and 2-DFM addition or 24 h after 2-FDG addition proving that all sugar analogs trigger ER stress and UPR activation (Figure 4). Moreover, Figure S3C showed how 2-DFM induced a more potent upregulation of BiP/GRP78 after 24 h of treatment than 2-DG and 2-FDG (Figure S3C).

3.5 | 2-DG, 2-FDG, and 2-DFM overcome KSHV-induced suppression of PERK downstream pathways in lytically reactivated cells

Before testing the impact of analog drugs on UPR activation in KSHV-infected cells, we first aimed to explore whether KSHV by itself induces UPR activation after lytic reactivation. The interplay between KSHV and UPR remains to be unraveled in iSLK cells. It was reported that KSHV induction activates all three UPR sensors but suppresses downstream transcriptional responses to support lytic replication in PEL cells.¹² We analyzed UPR activation by immunoblot and showed that KSHV switched on the PERK branch 24 h after lytic induction when the eIF2 α protein is phosphorylated (Figures 5A and S4A). Yet, neither ATF4 nor CHOP were upregulated (Figure 5A), suggesting that this pathway was being suppressed downstream by KSHV, as described previously by another research group.¹² KSHV-elicited suppression was so strong 24 h after lytic reactivation that it even inhibited the expression of ATF4 and CHOP triggered by Tg, a well-known inducer of UPR activation (Figure 5A). Regarding the other branch, IRE1 α seems to be activated after lytic induction, but its downstream effector sXBP1 was not upregulated (Figure 5A). Lastly, KSHV reactivation triggered the ATF6 branch since expression levels of the full-length ATF6 decreased over time (Figures 5A and S4A). Altogether, KSHV activates the PERK and IRE1 α branches but suppresses their downstream pathways in lytically induced cells. It also activates the ATF6 branch.

Our next goal was to examine the effect of sugar analogs in lytically reactivated cells. Not only are all three UPR sensors switched on after lytic reactivation and treatment, but also the drugs 2-DG and 2-DFM overcame KSHV-elicited inhibition of ATF4 and CHOP expression downstream of the PERK branch at 6 h (Figures 5B,D, and S5). 2-FDG also counteracted the expression impairment of ATF4 and CHOP

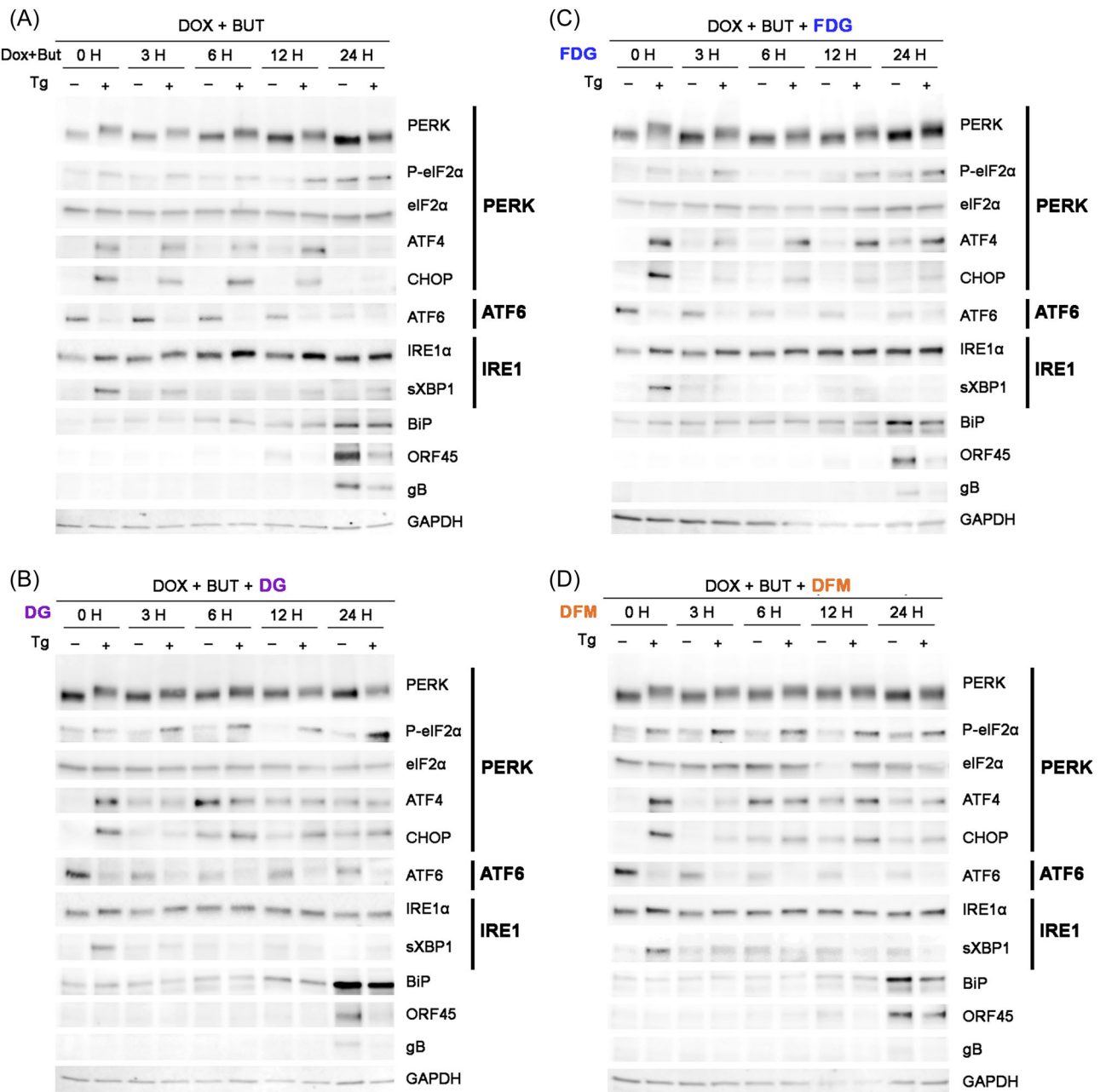


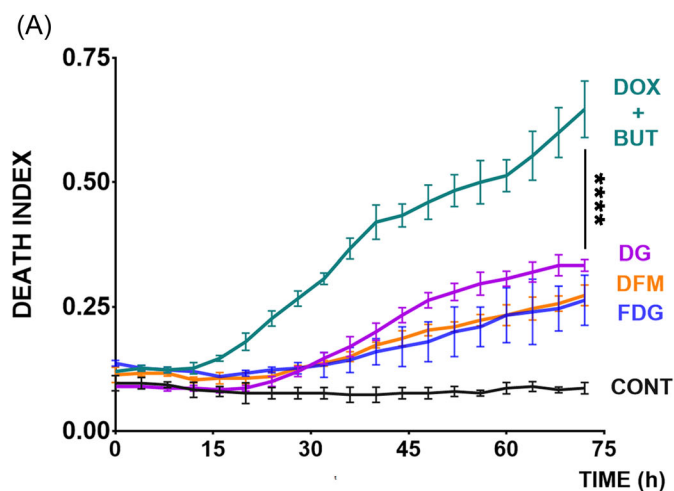
FIGURE 5 2-DG, 2-FDG, and 2-DFM surpass KSHV-elicited suppression of PERK downstream effectors in lytically reactivated cells. UPR markers (PERK, phospho- and total eIF2 α , ATF4, CHOP, full-length ATF6, IRE1 α , sXBP-1, and BiP) were analyzed. Migration shift in PERK and IRE1 α immunoblots correspond to phosphorylation. KSHV proteins ORF45 and gB were probed to indicate induction of early lytic and late lytic phases, respectively. GAPDH was used as a loading control. (A) Whole-cell lysates from induced iSLK.219 cells were analyzed by immunoblots for UPR and KSHV protein markers at different hours post-induction upon the addition of doxycycline (1 μ g/ml) and sodium butyrate (1 mM) (DOX + BUT). As a positive control of UPR activation, cells were treated with 150 nM thapsigargin (Tg) for 4 h before harvest. (B–D) Whole-cell lysates from reactivated iSLK.219 cells were analyzed by immunoblots for UPR and KSHV protein markers at different hours postinduction and posttreatment upon addition of doxycycline (1 μ g/ml) and sodium butyrate (1 mM) (DOX + BUT) along with 2-DG (B), 2-FDG (C), or 2-DFM (D) at 5 mM. As a positive control of UPR activation, cells were treated with 150 nM Tg for 4 h before harvest. ATF6, activating transcription factor 6; BiP, binding immunoglobulin protein; CHOP, C/EBP homologous protein; GAPDH, glyceraldehyde-3-phosphate dehydrogenase; KSHV, Kaposi's sarcoma-associated herpesvirus; PERK, protein kinase R-like endoplasmic reticulum kinase; UPR, unfolded protein response; 2-DG, 2-deoxy-D-glucose; 2-DFM, 2-deoxy-2-fluoro-D-mannose; 2-FDG, 2-fluoro-deoxy-D-glucose.

triggered by KSHV, but to a lesser extent than 2-DG and 2-DFM (Figures 5C and 5S). Additionally, eIF2 α was still phosphorylated 24–48 h after reactivation in all drug-treated cells (Figures 5B–D, and 54). In contrast, the occurrence of the transcription factor sXBP1 after IRE1 α activation is less clear, and only 2-DFM seems to surpass the expression inhibition of this effector. Finally, ATF6 was similarly activated in both untreated and drug-treated cells after lytic reactivation (Figures 5B–D and 54).

3.6 | Treatment with the sugar analogs 2-DG, 2-FDG, and 2-DFM protects lytically reactivated cells from dying

We next interrogated the cellular fate of reactivated cells treated with sugar analog drugs. Infected cells going through full viral replication eventually undergo apoptosis.²⁹ Alternatively, ER stress and UPR activation can lead to either apoptosis or autophagy, which can be pro-survival.³⁰ We examined the rate of cell death using the BAC16-transfected iSLK cell line, which expresses a GFP reporter (infection marker), and a Cytotox Red Reagent that assesses cell membrane integrity and, thus, enables to identify of dead cells. Using an IncuCyte[®] machine, which allows us to quantify fluorescent cells in real-time, we determined the death index (Figures 6A and 56). Surprisingly, the three sugar analogs partially protected reactivated cells from dying (Figures 6A and 56).

We also analyzed the expression of apoptotic markers (phospho-P53 and P53 and cleaved caspase 3) 48 h after lytic reactivation.



Nontreated reactivated cells presented increased levels of phospho-P53 and cleaved caspase 3 compared with their treated counterparts (Figure 6B). Conversely, the autophagy marker LC3B type II presented higher expression levels in those cells treated with the sugar analogs (Figure 6B, LC3B type II).

Altogether, 2-DG, 2-FDG, and 2-DFM play a protective role by blocking the cell death elicited by KSHV lytic replication. It was somehow expected that the analog drugs impair cell death because major viral glycoprotein synthesis is disrupted; therefore, lytic replication cannot be completed.

3.7 | Sugar analogs induce autophagy in lytically reactivated iSLK.219 cells

We hypothesized that the sugar analogs would prevent cell death in lytically reactivated cells by promoting autophagy, recognized as a major pro-survival mechanism that counteracts excessive UPR signaling. It was reported that 2-DG upregulates autophagy mainly through ER stress/UPR activation, playing a protective role against 2-DG-elicited cell death by relieving ER stress.³¹ Additionally, autophagy has been associated with increased levels of ATF4 and CHOP,³² and we previously demonstrated that the analog drugs enabled ATF4 and CHOP expression by overcoming KSHV-elicited inhibition (Figure 5B–D).

We showed that 2-DG, 2-FDG, and 2-DFM triggered autophagy 24 h after treatment with immunofluorescence using the autophagy marker LC3B (Figure 7). Reactivated cells (nontreated) did not show

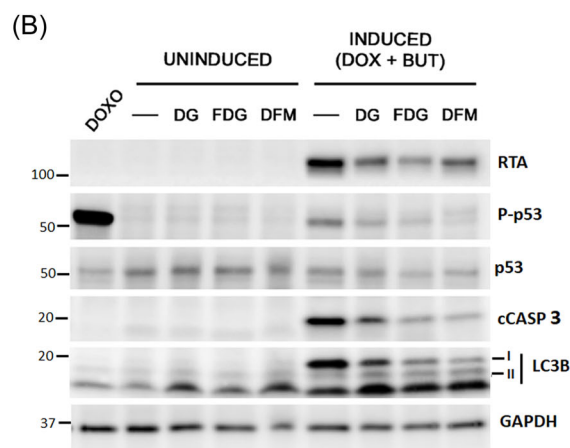


FIGURE 6 Treatment with 2-DG, 2-FDG, and 2-DFM protects lytically reactivated cells from dying through apoptosis. (A) The number of dead cells of noninduced (CONT) and lytically induced (DOX + BUT) iSLK.Bac16 cells treated with 2-DG, 2-FDG, or 2-DFM (5 mM) were counted over time using the Cytotox Red Reagent (250 nM) and the IncuCyte[®] machine, which allows for real-time cell quantification. Death index was calculated for each data point with the formula: Red object count (dead cells)/green object count (iSLK.Bac16 cells). Values were performed in triplicates and presented as means \pm SD (**** p < 0.0001; one-way ANOVA and Dunnett's multiple comparisons test). (B) Whole-cell lysates from reactivated iSLK.219 cells were analyzed by immunoblots for apoptotic markers (phospho-p53 and cCASP3) and the autophagy marker LC3B 48 h postinduction/treatment upon addition of doxycycline (1 μ g/ml) and sodium butyrate (1 mM) (DOX + BUT) alone (–) or in the presence of one of the sugar analogs: 2-DG, 2-FDG, or 2-DFM at 5 mM. Doxorubicin (DOXO) at 1 μ g/ml was used as a positive control of apoptotic markers. GAPDH, glyceraldehyde-3-phosphate dehydrogenase; 2-DG, 2-deoxy-D-glucose; 2-DFM, 2-deoxy-2-fluoro-D-mannose; 2-FDG, 2-fluoro-deoxy-D-glucose.

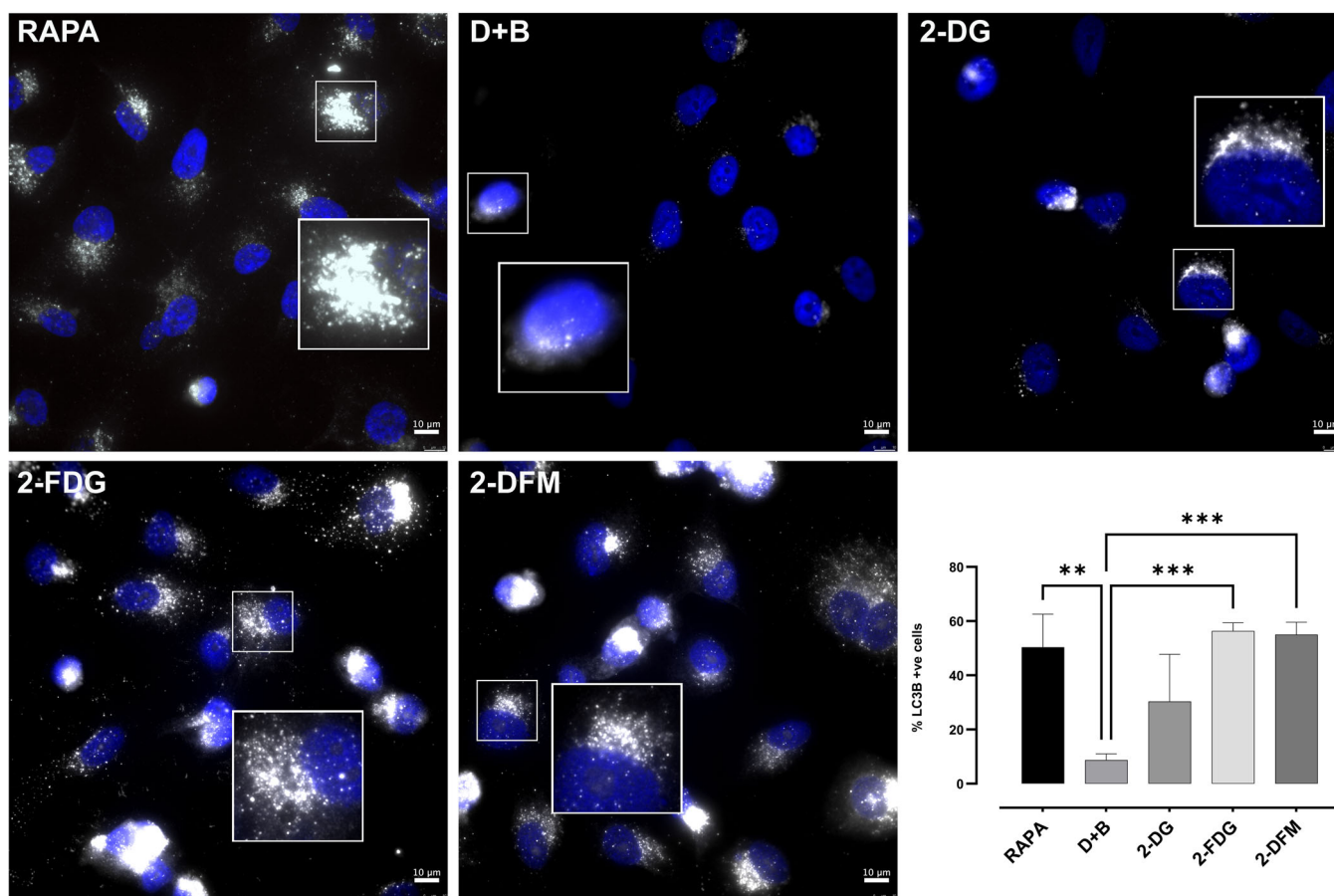


FIGURE 7 Treatment with 2-DG, 2-FDG, and 2-DFM induces autophagy in lytically reactivated iSLK.219 cells. Representative immunofluorescence pictures (63X) using the autophagy marker LC3B antibody, 24 h postinduction/treatment upon addition of doxycycline (1 μ g/ml) and sodium butyrate (1 mM) in the absence (D + B) or in presence of one of the sugar analogs: 2-DG, 2-FDG, or 2-DFM at 5 mM. Cells treated with rapamycin (Rapa) for 12 h were used as a positive control of autophagy. The nucleus was stained with DAPI. The percentage of LC3B-positive cells (considered when the area of LC3B label was $\geq 26 \mu\text{m}^2$ using Image J) was quantified in 50–110 cells per field per condition, in duplicate in 3 independent experiments. Error bars represent SD (** $p < 0.01$, *** $p < 0.001$). Differences among groups were analyzed using one-way ANOVA. ANOVA, analysis of variance; 2-DG, 2-deoxy-D-glucose; 2-DFM, 2-deoxy-2-fluoro-D-mannose; 2-FDG, 2-fluoro-deoxy-D-glucose.

the dotted signal as the one displayed in the treated cells. This confirms that the cellular fate of the host cell where KSHV undergoes lytic replication switches to autophagy following treatment with the analog drugs. A summary of our findings is summarized in the diagram in Figure 8.

4 | DISCUSSION

We found that 2-DG, 2-FDG, and 2-DFM inhibit KSHV replication and virion production at doses similar to those clinically achievable with 2-DG. Moreover, our data show that 2-DFM is the most potent antiviral compound pointing to *N*-glycosylation inhibition as the most critical target. Drug-induced suppression of *N*-glycosylation leads to ER stress, and activation of the cellular UPR, which, in turn, triggers autophagy protecting the host cell from KSHV-elicited apoptosis (Figure 8). Additionally, we showed that a stressed ER could no longer

support KSHV viral translational demands to produce structural glycoproteins (K8.1 and gB) that need to be mass-produced after lytic reactivation to generate progeny virions. We propose that sugar analogs such as 2-DG and the newly identified 2-DFM can be developed as clinically sound antivirals.

We found that *N*-glycosylation was impaired by the three analog drugs using D-mannose rescue experiments. D-mannose is one of the main components of the 14-sugar precursor that is added cotranslationally during folding and *N*-glycosylation in the ER. Both 2-DG and 2-DFM mimic this sugar and directly inhibit this mechanism. 2-FDG, on the other hand, only affects *N*-glycosylation indirectly due to its resemblance to D-glucose. The addition of D-mannose reversed lower expression levels of K8.1 and gB and fully rescued diminished virus titers in all drug-treated cells.

Drugs that interfere with *N*-glycosylation induce UPR increasing the protein folding capacity in the ER by upregulating chaperones such as BiP/GRP78.³³ In uninfected cells, BiP was upregulated 12 h after the

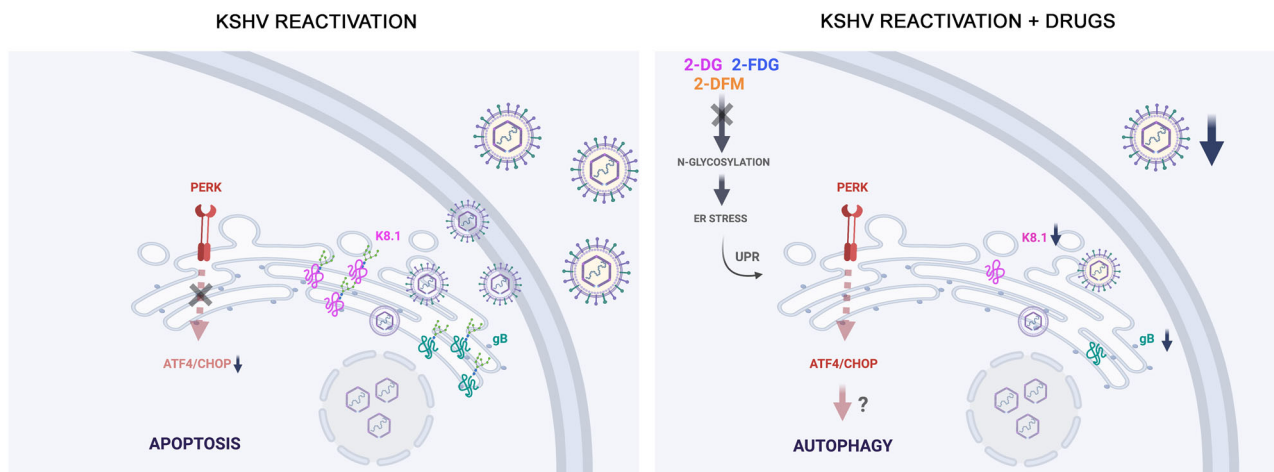


FIGURE 8 Diagram illustrating the effect of sugar analogs on KSHV replication through N-glycosylation inhibition and UPR activation. Left: During KSHV lytic replication, viral structural glycoproteins (K8.1 and gB) are mass-produced in the ER leading to UPR activation, including the PERK branch. However, KSHV inhibits the expression of PERK downstream effectors ATF4/CHOP. After virion production, the host cells undergo apoptosis. Right: Sugar analogs induce N-glycosylation inhibition leading to ER stress and activation of UPR. Consequently, K8.1 and gB expression are downregulated, and virion production is interrupted with fewer KSHV virus particles in supernatants. Additionally, sugar drugs counteract KSHV-elicited inhibition of ATF4/CHOP expression, which may favor autophagy over KSHV-induced apoptosis, protecting the host cell from dying. KSHV, Kaposi's sarcoma-associated herpesvirus; PERK, protein kinase R-like endoplasmic reticulum kinase; UPR, unfolded protein response; 2-DG, 2-deoxy-D-glucose; 2-DFM, 2-deoxy-2-fluoro-D-mannose; 2-FDG, 2-fluoro-deoxy-D-glucose.

treatment with 2-DG and 2-DFM and 24 h with 2-FDG. Also, sugar analogs activated two of the three branches of UPR with their downstream effectors: the PERK/ATF4/CHOP pathway and the IRE1 α /sXBP1 pathway (Figures 4 and S3). Surprisingly, eIF2 α was not phosphorylated by PERK, indicating that an alternative factor might mediate between PERK and the ATF4/CHOP effectors, such as eIF2A.¹²

KSHV also triggers UPR pathways during the lytic cycle. In PEL cells, lytic reactivation turns on UPR sensors but suppresses downstream transcriptional responses to support virus replication.¹² The authors propose that suppressing ATF6/sXBP1 transcription could prevent ERAD-mediated degradation of viral glycoproteins, and suppressing ATF4 and CHOP accumulation may allow KSHV to evade the adverse catabolic effects of autophagy.¹² Our work showed that KSHV activates all three branches of UPR in lytically reactivated iSLK cells. PERK activation led to eIF2 α phosphorylation 24 h after lytic induction (Figures 5A and S4A), likely due to viral manipulation to silence cellular bulk translation and favor KSHV glycoprotein expression. Alternatively, PERK branch activation could result from a significant burden in the ER generated by mass viral glycoprotein production since gB is already expressed at that time point (Figure 4A). Downregulation of the full-length ATF6 indicates that this pathway is also triggered by KSHV lytic replication. Finally, it is not clear whether IRE1 α is activated, although it seems to be triggered 6 h after lytic induction. Activation of UPR pathways at specific time points suggests that some viral genes could be involved. Moreover, expression of the PERK downstream effectors ATF4/CHOP was suppressed entirely, supporting previous evidence of KSHV inhibition of UPR downstream transcription factors. KSHV also inhibited sXBP1s expression (downstream of the IRE1 α branch) after lytic reactivation in cells treated with Tg.

When we studied the combined effects of sugar analogs and KSHV lytic induction on UPR, we observed that 2-DG, 2-DFM, and 2-FDG counteracted KSHV-elicited inhibition of ATF4/CHOP expression; although the latter drug at a lesser extent (Figure 5B–D). 2-FDG's milder effect can be explained by its lower potency on N-glycosylation inhibition. Other groups also reported that UPR induction by 2-DG, but not by 2-FDG, led to a significant upregulation of CHOP expression.³⁴ eIF2 α was not phosphorylated until 24 h after lytic induction, but phosphorylation by other kinases (general control nonderepressible-2; heme regulated inhibitor; and the IFN-induced kinase PKR) cannot be ruled out.

The interplay between KSHV and the host UPR leads to a different cellular outcome in the presence of the sugar analogs. KSHV-infected cells undergoing full viral replication eventually undergo apoptosis.²⁹ Indeed, we observed that lytically reactivated cells displayed increased expression of phospho-p53 and cleaved caspase 3 (Figure 6B). Conversely, in the presence of the analog drugs, these same cells downregulated these apoptotic markers and upregulated the autophagy marker LC3B type II (Figures 6B and 7). Additionally, real-time evaluation of cell membrane integrity, which allowed us to measure the cell death rate, indicated that sugar analogs play a protective role against KSHV-elicited cell death. Two feasible and complementary theories could explain these results. First, KSHV cannot produce virions in drug-treated cells, so apoptosis is impaired. Typically, induction of p53-mediated apoptosis is postponed by the activity of several proteins expressed during the earliest phases of viral replication to forestall early cell death and optimize virion production.²⁹ Alternatively, sugar analogs may favor autophagy, recognized as a major prosurvival mechanism that counteracts excessive UPR signaling.^{30,35} It was reported that 2-DG increases autophagy mainly through ER stress/UPR activation.³¹ We believe that

2-DG, 2-FDG, and 2-DFM could trigger autophagy by avoiding KSHV-elicited ATF4/CHOP suppression. It was proposed that inhibition of ATF4 and CHOP accumulation may allow KSHV to evade the adverse catabolic effects of autophagy since this mechanism compensates and assists ERAD with bulk protein degradation.¹²

2-DG is the most clinically developed drug and has proven to be safe at 63 mg/kg/day in combination with docetaxel with tolerable adverse effects in a phase I trial in patients with advanced solid tumors.³⁶ In a randomized, open-label, phase II clinical trial using 45 mg/kg two times per day, 2-DG, which is available in powder form in sachets for oral route administration as an adjunct therapy, was found to be safe and effective in COVID-19 patients and showed to significantly improve their recovery, which resulted in its emergency approval to help control SARS-CoV-2 infection in India.^{16,37} The Drugs Controller General of India cleared the drug after clinical trial results showed that 2-DG promotes the faster recovery of hospitalized patients and lower supplemental oxygen dependence as an adjunct therapy. 2-DG is also the most versatile drug blocking viral infections in nonenveloped viruses, such as rhinovirus 14, and enveloped viruses, such as KSHV⁸ and porcine epidemic diarrhea virus, an alpha coronavirus.³⁸ Stoichiometrically, 2-DG should predominantly interfere with D-mannose metabolism at 1–2 mM and at doses above 5–6 mM, it should effectively inhibit the utilization of both sugar isomers (D-mannose and D-glucose).^{39,40}

D-glucose concentration in serum ranges between 4 and 6 mM, while D-mannose concentrations are usually at 100 μM or below. This fact would explain why 2-DFM could be the most potent drug in vivo. Previously, 2-DFM was found to be less effective than 2-DG in interfering with lipid-linked oligosaccharides assembly because 2-DG, but not 2-DFM, incorporated into the oligosaccharide chain.²² However, in those studies the potency of inducing ER stress and activating the UPR of these analogs was not tested. Moreover, as previously reported by the Lampidis group that 2-DG was more potent than 2-DFM in killing select tumor cells under normoxic conditions, the magnitude of these two analogs to induce ER stress was not discussed in regard to toxic potencies. A possible explanation as to why viral titer is more sensitive to 2-DFM than 2-DG may be that in cancer cells the increased potency of 2-DFM versus 2-DG to induce ER stress augments the induction of autophagy more by 2-DFM than 2-DG (as shown in Figure 7) which in cancer cells is protective. Thus, for viral replication in cells that we show here are not affected by the toxic effects of ER stress, 2-DFM's more potent induction of ER stress and UPR activation (shown by BiP upregulation, Figure S3C) would explain its enhanced inhibition of viral replication as compared with 2-DG's.

The present study confirmed that 2-DG effectively blocked virus replication and demonstrated the protective role of the three analogs against KSHV-induced cell death. Their ability to favor autophagy over apoptosis is essential when tissue damage needs to be avoided. Moreover, our data support the therapeutic potential of 2-DFM as a potent and specific antiviral agent. As a D-mannose analog, it exerts its effect at lower concentrations than D-glucose-based drugs. Finally, we identified the nontoxic inhibition of N-glycosylation as a critical target to impair virion production of KSHV and, potentially, other

enveloped viruses such as SARS-CoV-2. Our contributions to better understanding the mechanism of action of sugar analogs will offer new avenues for innovative therapies.

IN MEMORIAM

Dr. Enrique A. Mesri, an inspiring scientist, a great mentor, and friend, who sadly passed away days before sending the manuscript. For his dedication and contributions to the KSHV and viral oncology field, we will always be in debt to him.

AUTHOR CONTRIBUTIONS

Conceptualization, data curation, formal analysis, methodology, validation, visualization, investigation, writing-original draft, writing-review, and editing: Mariana Schlesinger. Data curation, formal analysis, methodology, validation, and investigation: Christian McDonald. Data curation, formal analysis, methodology, validation, and investigation: Anuj Ahuja. Data curation, formal analysis, methodology, validation, and investigation: Carolina Alejandra Alvarez Canete. Data curation, formal analysis, methodology, validation, and investigation: Zelmira Nuñez del Prado. Data curation, formal analysis, investigation, writing-original draft, writing-review, and editing: Julian Naipauer. Conceptualization, investigation, supervision, formal analysis, and methodology: Theodore Lampidis. Conceptualization, data curation, methodology, investigation, writing-original draft, writing-review and editing, supervision, funding acquisition, and project administration: Enrique A. Mesri.

ACKNOWLEDGMENTS

We want to thank Dr. Omayra Méndez-Solís for her constant assistance with experimental design and troubleshooting of experiments, Dr. Julia Martinez for her assistance with the Incucyte live cell analysis system, supported by shared equipment funds provided by the Sylvester Comprehensive Cancer Center, and Dr. Celina Amaya and Dr. Ramiro Verdun for their help and assistance with the microscopy techniques. Also, we would like to thank the Flow Cytometry Core Facility members, especially Patricia Guevara, for their assistance with Flow Cytometry and cell sorting analysis. This work was funded by NIH grant CA136387.

CONFLICT OF INTERESTS

Theodore J. Lampidis is an unpaid member of the scientific advisory board of G.ST Antivirals, a startup company in Vienna, Austria, that is developing the delivery of 2-DG via nasal spray for rhinoviral infections. The University of Miami, where Dr. Lampidis is employed, has signed a collaborative contract with G.ST Antivirals. The other authors declare no conflict of interests.

DATA AVAILABILITY STATEMENT

The data sets generated during and/or analyzed during the current study are available from the corresponding author on reasonable request. The data that support the findings of this study are available from the corresponding author upon reasonable request.

ORCID

Anuj Ahuja  <http://orcid.org/0000-0002-0558-1356>Julian Naipauer  <http://orcid.org/0000-0001-6842-6815>

REFERENCES

- Mesri EA, Cesarman E, Boshoff C. Kaposi's sarcoma and its associated herpesvirus. *Nat Rev Cancer*. 2010;10(10):707-719.
- Dissinger NJ, Damania B. Recent advances in understanding Kaposi's sarcoma-associated herpesvirus. *F1000Research*. 2016;5:740.
- Cesarman E, Damania B, Krown SE, Martin J, Bower M, Whitby D. Kaposi sarcoma. *Nat Rev Dis Primers*. 2019;5(1):9.
- Montaner S, Sodhi A, Molinolo A, et al. Endothelial infection with KSHV genes in vivo reveals that vGPCR initiates Kaposi's sarcoma-genesis and can promote the tumorigenic potential of viral latent genes. *Cancer Cell*. 2003;3(1):23-36.
- Cavallin LE, Ma Q, Naipauer J, et al. KSHV-induced ligand mediated activation of PDGF receptor- α drives Kaposi's sarcomagenesis. *PLoS Pathog*. 2018;14(7):e1007175.
- Krishnan HH, Sharma-Walia N, Zeng L, Gao SJ, Chandran B. Envelope glycoprotein gB of Kaposi's sarcoma-associated herpesvirus is essential for egress from infected cells. *J Virol*. 2005;79(17):10952-10967.
- Zhu FX, Chong JM, Wu L, Yuan Y. Virion proteins of Kaposi's sarcoma-associated herpesvirus. *J Virol*. 2005;79(2):800-811.
- Leung HJ, Duran EM, Kurtoglu M, Andreansky S, Lampidis TJ, Mesri EA. Activation of the unfolded protein response by 2-deoxy-D-glucose inhibits Kaposi's sarcoma-associated herpesvirus replication and gene expression. *Antimicrob Agents Chemother*. 2012;56(11):5794-5803.
- Cheng G, Feng Z, He B. Herpes simplex virus 1 infection activates the endoplasmic reticulum resident kinase PERK and mediates eIF-2 α dephosphorylation by the γ 134.5 protein. *J Virol*. 2005;79(3):1379-1388.
- He B. Viruses, endoplasmic reticulum stress, and interferon responses. *Cell Death Differ*. 2006;13(3):393-403.
- Isler JA, Skalet AH, Alwine JC. Human cytomegalovirus infection activates and regulates the unfolded protein response. *J Virol*. 2005;79(11):6890-6899.
- Johnston BP, Pringle ES, McCormick C. KSHV activates unfolded protein response sensors but suppresses downstream transcriptional responses to support lytic replication. *PLoS Pathog*. 2019;15(12):e1008185.
- Delgado T, Carroll PA, Punjabi AS, Margineantu D, Hockenbery DM, Lagunoff M. Induction of the Warburg effect by Kaposi's sarcoma herpesvirus is required for the maintenance of latently infected endothelial cells. *Proc Natl Acad Sci USA*. 2010;107(23):10696-10701.
- Gualdoni GA, Mayer KA, Kapsch AM, et al. Rhinovirus induces an anabolic reprogramming in host cell metabolism essential for viral replication. *Proc Natl Acad Sci USA*. 2018;115(30):E7158-E7165.
- Karabajakian A, Ray-Coquard I, Blay JY. Molecular mechanisms of Kaposi sarcoma development. *Cancers*. 2022;14(8):1869.
- Mesri EA, Lampidis TJ. 2-Deoxy-d-glucose exploits increased glucose metabolism in cancer and viral-infected cells: relevance to its use in India against SARS-CoV-2. *IUBMB Life*. 2021;73(10):1198-1204.
- Bojkova D, Klann K, Koch B, et al. Proteomics of SARS-CoV-2-infected host cells reveals therapy targets. *Nature*. 2020;583(7816):469-472.
- Lampidis TJ, Kurtoglu M, Maher JC, et al. Efficacy of 2-halogen substituted D-glucose analogs in blocking glycolysis and killing "hypoxic tumor cells". *Cancer Chemother Pharmacol*. 2006;58(6):725-734.
- Siddiquey MNA, Zhang H, Nguyen CC, Domma AJ, Kamil JP. The human cytomegalovirus endoplasmic reticulum-resident glycoprotein UL148 activates the unfolded protein response. *J Virol*. 2018;92(20):e00896-e00918.
- Kurtoglu M, Maher JC, Lampidis TJ. Differential toxic mechanisms of 2-deoxy-D-glucose versus 2-fluorodeoxy-D-glucose in hypoxic and normoxic tumor cells. *Antioxid Redox Signal*. 2007;9(9):1383-1390.
- Datema R, Schwarz RT. Interference with glycosylation of glycoproteins. *Biochem J*. 1979;184(1):113-123.
- Datema R, Schwarz RT, Jankowski AW. Fluoroglucose-inhibition of protein glycosylation in vivo. Inhibition of mannose and glucose incorporation into lipid-linked oligosaccharides. *Eur J Biochem*. 1980;109(2):331-341.
- Schmidt MFG, Schwarz RT, Scholtissek C. Nucleoside-diphosphate derivatives of 2-deoxy-D-glucose in animal cells. *Eur J Biochem*. 1974;49(1):237-247.
- Vieira J, O'Hearn PM. Use of the red fluorescent protein as a marker of Kaposi's sarcoma-associated herpesvirus lytic gene expression. *Virology*. 2004;325(2):225-240.
- Brulois KF, Chang H, Lee ASY, et al. Construction and manipulation of a new Kaposi's sarcoma-associated herpesvirus bacterial artificial chromosome clone. *J Virol*. 2012;86(18):9708-9720.
- Brulois K, Toth Z, Wong LY, et al. Kaposi's sarcoma-associated herpesvirus K3 and K5 ubiquitin E3 ligases have stage-specific immune evasion roles during lytic replication. *J Virol*. 2014;88(16):9335-9349.
- Myoung J, Ganem D. Generation of a doxycycline-inducible KSHV producer cell line of endothelial origin: maintenance of tight latency with efficient reactivation upon induction. *J Virol Methods*. 2011;174(1-2):12-21.
- Johnston BP, McCormick C. Herpesviruses and the unfolded protein response. *Viruses*. 2019;12(1):17.
- Moore PS. KSHV manipulation of the cell cycle and apoptosis. In: Arvin A, Campadelli-Fiume G, Mocarski E, et al., eds. *Human Herpesviruses: Biology, Therapy, and Immunoprophylaxis*, 2007.
- Chakrabarti A, Chen AW, Varner JD. A review of the mammalian unfolded protein response. *Biotechnol Bioeng*. 2011;108(12):2777-2793.
- Xi H, Kurtoglu M, Liu H, et al. 2-Deoxy-D-glucose activates autophagy via endoplasmic reticulum stress rather than ATP depletion. *Cancer Chemother Pharmacol*. 2011;67(4):899-910.
- Sano R, Reed JC. ER stress-induced cell death mechanisms. *Biochim Biophys Acta - Mol Cell Res*. 2013;1833(12):3460-3470.
- Kurtoglu M, Gao N, Shang J, et al. Under normoxia, 2-deoxy-D-glucose elicits cell death in select tumor types not by inhibition of glycolysis but by interfering with N-linked glycosylation. *Mol Cancer Ther*. 2007;6(11):3049-3058.
- Merchan JR, Kovács K, Railsback JW, et al. Antiangiogenic activity of 2-deoxy-D-glucose. *PLoS One*. 2010;5(10):e13699.
- Acharya BR, Bhattacharyya S, Choudhury D, Chakrabarti G. The microtubule depolymerizing agent naphthazarin induces both apoptosis and autophagy in A549 lung cancer cells. *Apoptosis*. 2011;16(9):924-939.
- Raez LE, Papadopoulos K, Ricart AD, et al. A phase I dose-escalation trial of 2-deoxy-D-glucose alone or combined with docetaxel in patients with advanced solid tumors. *Cancer Chemother Pharmacol*. 2013;71(2):523-530.
- Bhatt AN, Shenoy S, Munjal S, et al. 2-deoxy-D-glucose as an adjunct to standard of care in the medical management of COVID-19: a proof-of-concept and dose-ranging randomised phase II clinical trial. *BMC Infect Dis*. 2022;22(1):669.
- Wang Y, Li J, Sun M, et al. Triggering unfolded protein response by 2-Deoxy-D-glucose inhibits porcine epidemic diarrhea virus propagation. *Antiviral Res*. 2014;106:33-41.
- Etchison JR, Freeze HH. Enzymatic assay of D-mannose in serum. *Clin Chem*. 1997;43(3):533-538.

40. Xi H, Kurtoglu M, Lampidis TJ. The wonders of 2-deoxy-D-glucose. *IUBMB Life*. 2014;66(2):110-121.

SUPPORTING INFORMATION

Additional supporting information can be found online in the Supporting Information section at the end of this article.

How to cite this article: Schlesinger M, McDonald C, Ahuja A, et al. Glucose and mannose analogs inhibit KSHV replication by blocking *N*-glycosylation and inducing the unfolded protein response. *J Med Virol*. 2022;e28314. doi:10.1002/jmv.28314